Internalization of erythrocyte acylpeptide hydrolase is required for asexual replication of *Plasmodium falciparum*

Rubayet Elahi, Christie Dapper, Michael Klemba#

Department of Biochemistry, Virginia Tech, Blacksburg, Virginia, USA

Running Head: Human acylpeptide hydrolase in *P. falciparum*

#Address correspondence to Michael Klemba, klemba@vt.edu.

Abstract word count: 233

Text word count: 4,675

ABSTRACT

The human malaria parasite *Plasmodium falciparum* causes disease as it replicates within the host's erythrocytes. We have found that an erythrocyte serine hydrolase, acylpeptide hydrolase (APEH), accumulates within developing asexual parasites. Internalization of APEH was associated with a proteolytic event that reduced the size of the catalytic polypeptide from 80 to 55 kDa, which suggests that the enzyme resides in the food vacuole. A triazole urea APEH inhibitor, termed AA74-1, was employed to characterize the role of parasite-internalized APEH. *In vitro*, AA74-1 was a potent and highly selective inhibitor of both host erythrocyte and parasite-internalized APEH. When added to cultures of parasite-infected erythrocytes, AA74-1 was a relatively poor inhibitor of replication over one asexual replication cycle; however, its potency increased dramatically after a second cycle. This enhancement of potency was not abrogated by the addition of exogenous isopentenyl pyrophosphate, which distinguishes it from the well-characterized "delayed death" phenomenon that is observed with inhibitors that target the parasite apicoplast. Analysis of inhibition by AA74-1 *in vivo* revealed that a concentration of 100 nM was sufficient to quantitatively inhibit erythrocyte APEH. In contrast, the parasite-internalized APEH pool was inefficiently inhibited at concentrations up to 100-fold higher. Together, these findings provide evidence for an essential catalytic role for parasite-internalized APEH and suggest a model for AA74-1 growth inhibition whereby depletion of parasite APEH activity requires the internalization of inactive host cell APEH over two replication cycles.

48 **IMPORTANCE**

49 Nearly half a million deaths were attributed to malaria in 2017. Protozoan parasites of the genus
50 *Plasmodium* cause disease in humans while replicating asexually within the host's erythrocytes,
51 with *P. falciparum* responsible for most of the mortality. Understanding how *Plasmodium* spp.
52 has adapted to its unique host erythrocyte environment is important for developing malaria
53 control strategies. Here, we demonstrate that *P. falciparum* co-opts a host erythrocyte serine
54 hydrolase termed acylpeptide hydrolase. By showing that the parasite requires acylpeptide
55 hydrolase activity for replication, we expand our knowledge of host cell factors that contribute to
56 robust parasite growth.

57

58 **KEY WORDS:** Plasmodium, malaria, erythrocyte, serine hydrolase, acylpeptide hydrolase

59

60

INTRODUCTION

In 2017, an estimated US $3.1 billion was spent on malaria control worldwide. Despite this expenditure, around half a million deaths due to malaria were reported that year (1). *Plasmodium falciparum*, one of the five species that cause human malaria, accounts for the vast majority of these deaths (1). While still unacceptably large, the latest mortality figure represents a substantial improvement on the malaria situation of fifteen years ago, which is due in part to the implementation of artemisinin combination therapy (2). Recent reports of reduced efficacy in Southeast Asia have raised concerns that parasites are evolving resistance (or tolerance) to artemisinins and their partner drugs (3, 4). The discovery and validation of new anti-malarial targets is therefore a critical component of a robust anti-malarial pipeline, which is needed to safeguard recent advances and to devise strategies for eradication.

Enzymes of the serine hydrolase superfamily encompass a highly diverse range of catalytic activities and have garnered much attention for their roles in many critical metabolic processes in humans (5, 6). Based on annotated sequence homologies, the *P. falciparum* genome encodes over 40 putative members of the serine hydrolase superfamily (7), most of which have not been functionally characterized. Exploration of the roles of uncharacterized serine hydrolases will lead to new insights into essential aspects of parasite metabolism and possibly to new chemotherapeutic targets.

Serine hydrolase-directed activity-based probes (ABPs) have emerged as powerful tools for the functional annotation of serine hydrolases in complex proteomes (5, 8). By enabling competitive activity-based protein profiling (ABPP), ABPs have greatly accelerated the discovery of inhibitors that are highly specific for individual serine hydrolases (5). ABPs containing a fluorophosphonate (FP) warhead provide broad coverage of the serine hydrolase

84 superfamily with negligible off-target activity (9, 10). Reaction of the FP warhead with the active
85 site serine forms a stable covalent adduct. ABPs containing a fluorescent reporter enable a direct
86 quantitative readout of the levels of active serine hydrolases (10).

87 We have employed a fluorescent FP probe in conjunction with well-characterized serine
88 hydrolase inhibitors to profile the serine hydrolase activities of asexual intraerythrocytic *P.*
89 *falciparum*. In the course of these studies, we made the surprising discovery that a human host
90 erythrocyte serine hydrolase, acylpeptide hydrolase (APEH, EC: 3.4.19.1; also referred to as
91 acylamino acid releasing enzyme and acylaminoacyl-peptidase) is one of the most abundant
92 serine hydrolases in the developing asexual parasite. APEH is a member of the prolyl
93 oligopeptidase (POP) family of serine peptidases (clan SC, family S9C). In mammals, APEH is
94 ubiquitously expressed (11) and it has been purified from human erythrocytes as a homotetramer
95 (12, 13). APEH was initially identified as an exopeptidase that catalyzes the hydrolysis of N-
96 terminally acylated amino acids from peptides, yielding an acylamino acid and a shortened
97 peptide with a free N-terminus (14, 15). Acetylated and formylated peptides are good substrates
98 for APEH (16, 17). There have also been reports of APEH endopeptidase activity against
99 oxidized proteins (18) and amyloidogenic Aβ peptide (19).

100 The physiological roles of APEH in mammalian cells are not completely understood. On
101 the basis of the exopeptidase activity of APEH noted above, it has long been hypothesized that
102 APEH participates in the maturation of proteins through the removal of acetylated N-terminal
103 residues (20). Treatment of mouse T cells with a potent and highly selective inhibitor of APEH,
104 termed AA74-1, affected the acetylation status of 25 proteins, lending support for this hypothesis
105 (21). There is some evidence that APEH influences activity of the proteasome (22, 23); however,
106 the mechanistic details of this interaction remain to be elucidated.

Here, we have employed the fluorescent activity-based serine hydrolase probe TAMRA-fluorophosphonate (TAMRA-FP), the covalent triazole urea APEH inhibitor AA74-1, and anti-APEH antibodies to explore the properties and physiological role of the parasite-internalized enzyme.

RESULTS

Identification of human APEH in saponin-isolated *P. falciparum*

As a first step towards a proteome-wide functional annotation of serine hydrolase activities in asexual *P. falciparum*, we compared the TAMRA-FP labeling profiles of crude lysates of uninfected erythrocytes and of saponin-isolated parasites (Fig. 1A). Saponin selectively permeabilizes the erythrocyte plasma membrane and the parasitophorous vacuole (PV) membrane of parasite-infected red blood cells; thus, saponin-treated parasites lack soluble erythrocyte and PV proteins (24). Unsurprisingly, there is little overlap between the two profiles, which is consistent with an organism-specific pattern of serine hydrolase expression.

To gain insight into the functionality of *P. falciparum* serine hydrolases, competitive activity-based probe profiling (referred to as competitive ABPP) was conducted. Crude lysates of saponin-isolated parasites were incubated with covalent inhibitors of diverse human serine hydrolases prior or vehicle (1% DMSO) prior to TAMRA-FP labeling (Fig. 1B; structures of inhibitors and their known targets are provided in Table S1). We were intrigued to find that AA74-1, a triazole urea inhibitor (Fig. 1C) that is highly selective for human APEH (21), completely blocked TAMRA-FP labeling of a major ~55 kDa species and a minor ~80 kDa species in parasite lysate (Fig. 1B). In contrast, lipase or fatty acid amide hydrolase inhibitors did not compete with labeling of the 55 or 80 kDa species (Fig. 1B). Treatment of erythrocyte lysate

with the same inhibitor panel revealed that AA74-1, but not lipase or fatty acid amide hydrolase inhibitors, blocked TAMRA-FP labeling of an ~80 kDa species in a highly selective manner (Figs. 1D, S1). The estimated molecular mass of this species is consistent with a predicted molecular mass of 81.2 kDa for human APEH (25).

The above findings suggest two possible interpretations: i) *P. falciparum* expresses an endogenous protein with activity similar to that of human APEH, or ii) the parasite internalizes the erythrocyte enzyme. To distinguish between these possibilities, we asked whether parasite-internalized APEH is recognized by an affinity purified anti-human APEH antibody (Fig. 1E). Parasite and erythrocyte lysates were first analyzed by competitive ABPP with and without AA74-1 to identify APEH (Fig. 1E). After in-gel fluorescence scanning of TAMRA-FP-labeled species, the proteins were transferred to nitrocellulose and APEH was detected by immunoblotting. The 80 kDa species in erythrocyte lysate and the major 55 kDa and minor 80 kDa species in parasite lysate were recognized by the antibody, with the relative abundance of the species on the membrane comparable to that observed in the TAMRA-FP scan (Fig. 1E). These findings strongly suggest that *P. falciparum* internalizes APEH, which then appears to undergo a proteolytic event to reduce the size of the active site-containing segment from 80 to 55 kDa. The minor ~80 kDa species in parasite lysate that is inhibited by AA74-1 likely represents full-length, uncleaved APEH. Hereafter, these two species will be collectively referred to as "parasite-internalized APEH".

Validation of AA74-1 as a potent and selective inhibitor of parasite-internalized APEH

Before using AA74-1 to probe the importance of internalized APEH for intraerythrocytic parasite development, we evaluated its potency and selectivity *in vitro*. The 50% inhibitory

153 concentration (IC_{50}) values for AA74-1 inhibition of erythrocyte and parasite-internalized APEH
154 were determined by competitive ABPP (Fig. 2A, B). Mean IC_{50} values from three independent
155 replicates were 7.9 ± 1.8 nM for the parasite 55 kDa species and 7.4 ± 2.4 nM for the erythrocyte
156 80 kDa species, which are not significantly different (two-tailed Student's *t*-test, *p*-value = 0.78).
157 These values are very close to the 11 nM IC_{50} value reported for AA74-1 inhibition of APEH in
158 a human cell line using a similar competitive ABPP assay (21). The parasite 80 kDa species
159 appeared to have a comparable IC_{50} value (Fig. 2A), but its lower abundance made it difficult to
160 reliably quantify this species.

161 To assess the selectivity of AA74-1 for APEH in saponin-isolated parasite lysate, the
162 fluorescence profiles of the lanes corresponding to 135 and 405 nM AA74-1 in Fig. 2A were
163 compared to that of the vehicle (DMSO) control (Fig. 2C). At both concentrations, the 80 and 55
164 kDa APEH species were effectively inhibited (Fig. 2C, red asterisks). A 37 kDa species was
165 partially inhibited at both concentrations. In separate studies, we have identified this species as
166 the "prodrug activation and resistance esterase" (R. Elahi, C. Dapper and M. Klemba,
167 unpublished data), a serine hydrolase that is not essential for asexual replication of *P. falciparum*
168 (31). We conclude that concentrations of AA74-1 below ~400 nM are highly selective for the 55
169 and 80 kDa species of APEH in saponin-isolated parasite lysate *in vitro*.
170
171 **The anti-malarial potency of AA74-1 is enhanced over two replication cycles**
172 To determine whether internalized APEH is required for efficient parasite replication, we
173 examined the effect of AA74-1 on the development of a synchronized ring-stage culture. Parasite
174 replication was assessed by measuring the fluorescence of the DNA-binding dye SYBR Green I
175 after 48 h (the time required for one complete cycle of the 3D7 line is ~42 h). AA74-1 was a

176 relatively poor inhibitor of parasite growth, with incomplete inhibition of parasite replication at
177 10 μM and an estimated 50% effective concentration (EC_{50}) greater than 1 μM (Fig. 3A, Table
178 1). Interestingly, however, when parasites were seeded at a lower density and allowed to proceed
179 through two replication cycles (96 h), the efficacy of AA74-1 increased by over 10-fold,
180 exhibiting a mean EC_{50} value of 96 ± 38 nM over three biological replicates (Fig. 3A, Table 1).
181 Near complete inhibition of parasite replication on the second cycle was observed at an AA74-1
182 concentration of 310 nM, a value that is highly selective for APEH *in vitro* (Fig. 2B). In contrast
183 to these results, parallel experiments with chloroquine yielded 48 and 96 hour EC_{50} values that
184 were not significantly different (Table 1; Student's two-tailed *t*-test, *p*-value = 0.93).
185 Dramatic enhancement of anti-malarial potency during a second replication cycle is a
186 hallmark of compounds that target the *P. falciparum* apicoplast (26, 27) and is referred to as
187 "delayed death". An apicoplast-based delayed death response can be reversed by
188 supplementation of parasite culture medium with 200 μM isopentenyl pyrophosphate (IPP),
189 which is the sole product of apicoplast metabolism that is required during the asexual growth
190 cycle (26). To determine whether the enhanced potency of AA74-1 might be due to inhibition of
191 an apicoplast enzyme, we conducted 96 hour growth assays in the presence and absence of 200
192 μM IPP. As a positive control for delayed death, parallel experiments were performed with
193 clindamycin, an antibiotic that targets the apicoplast. Clindamycin has been shown to exhibit a
194 profound delayed death response, which can be rescued by IPP supplementation (26, 27). While
195 clindamycin toxicity was dramatically attenuated in the presence of IPP (Fig. 3B, Table 1), the
196 potency of AA74-1 was unaffected (Fig. 3A, Table 1). These results strongly suggest that AA74-
197 1 does not target an apicoplast enzyme and indicate that an alternate mechanism lies behind the
198 enhancement of AA74-1 potency during the second replication cycle.

199

200 **Parasite-internalized APEH, but not erythrocyte APEH, is recalcitrant to AA74-1**

201 **inhibition *in vivo***

202 Seeking an explanation for the enhanced potency of AA74-1 during the second

203 replication cycle, we asked whether AA74-1 is an effective inhibitor of parasite-internalized

204 APEH *in vivo*. Because AA74-1 covalently modifies the active site serine of APEH (21), the

205 inhibitor can be added to parasite cultures for a defined period of time and the extent of APEH

206 inhibition *in vivo* can be assessed by TAMRA-FP labeling following inhibitor washout and

207 saponin isolation of parasites. We determined the amount of residual internalized APEH activity

208 following a four-hour treatment of cultured trophozoite-stage parasites with 0.1, 1 or 10 μM

209 AA74-1. A four-hour treatment window was selected in order to minimize the potentially

210 confounding effects of toxicity at the higher AA74-1 concentrations (Fig. 3A). Surprisingly,

211 parasite-internalized APEH was not effectively inhibited by exogenous AA74-1 concentrations

212 up to 10 μM (Fig. 4A). A parallel experiment with uninfected erythrocytes demonstrated robust

213 inhibition of APEH at all exogenous AA74-1 concentrations (Fig. 4A). These results indicate

214 that the inhibitor is able to diffuse across the erythrocyte plasma membrane but is unable to

215 inhibit APEH within the parasite.

216 To further explore this phenomenon, we conducted an experiment to determine whether

217 there was something distinctive about *P. falciparum*-infected erythrocytes that prevented

218 accumulation of AA74-1. Trophozoite-stage parasites were treated for four hours with 100 nM

219 exogenous AA74-1, washed extensively, and purified on a magnetic column to > 90%

220 parasitemia (this material is referred to as “pRBCs”). We then fractionated the pRBCs with

221 saponin, yielding a supernatant containing host erythrocyte APEH, and a pellet containing

parasite-internalized APEH. A schematic of the experimental design is shown in Fig. 4B. Once again, we observed inhibition of erythrocyte APEH but not parasitize-internalized APEH (Fig. 4B).

Parasite-internalized APEH is active and is inhibited by AA74-1 at acidic pH

The most likely scenario for internalization of host cell APEH is through the endocytosis of large quantities of erythrocyte cytosol and delivery to the food vacuole (see Discussion). The lumen of the food vacuole is acidic with a pH of ~ 5.5 (28, 29). To determine whether APEH could have a catalytic role at this pH, we asked whether TAMRA-FP modifies the active site serine of APEH at pH 5.5. While APEH was labeled with TAMRA-FP at pH 5.5 (Fig. 5), the extent of labeling was lower at pH 5.5 than at 7.4, which suggests a slower reaction rate at the acidic pH value. We also found that AA74-1 is capable of inhibiting APEH at pH 5.5 *in vitro* (Fig. 5); thus, an acidic pH does not by itself explain the recalcitrance of APEH to AA74-1 inhibition *in vivo*.

DISCUSSION

We present evidence that *P. falciparum* internalizes and accumulates erythrocyte APEH during its growth in the host cell. There are several reported examples of *P. falciparum* importing host cell proteins for metabolic purposes, including superoxide dismutase (30), δ-aminolevulinate dehydratase (31), and peroxiredoxin 2 (32). APEH is the first example to our knowledge of a hydrolytic enzyme accumulating in the parasite.

The most likely route for internalization of erythrocyte APEH is through the cytostomal endocytic pathway that is responsible for the uptake and delivery to the food vacuole of large

quantities of erythrocyte cytosol (33-35). Up to 75% of erythrocyte hemoglobin, the dominant constituent of erythrocyte cytosol, is internalized through this pathway (36). Because cytostomal endocytosis is thought to be a non-specific process, APEH would presumably be delivered to the food vacuole along with hemoglobin and other soluble erythrocyte proteins. This model for APEH internalization is consistent with the observed proteolysis of parasite APEH to a 55 kDa species, which may be mediated by vacuolar aspartic and cysteine endopeptidases (37). Our findings are consistent with those of several previous studies demonstrating that APEH is highly resistant to proteolytic degradation and that endoproteases such as trypsin, chymotrypsin and elastase clip full-length, 80 kDa APEH into ~55 kDa and ~25 kDa fragments *in vitro* (38-41). Interestingly, these studies have established that this proteolytic treatment neither disrupts the homotetrameric structure of APEH nor reduces its activity (38, 39), thus providing a plausible explanation for the stability of APEH in the proteolytic environment of the food vacuole. The shift in size of APEH in saponin-isolated parasite lysates indicates that it does not originate from contamination by host erythrocyte cytosol or from interaction with the outer leaflet of the parasite plasma membrane. We have tried to confirm a food vacuole location for APEH through indirect immunofluorescence using anti-APEH antibodies; however, although we have tested a wide range of fixation conditions and numerous antibodies, we have not found conditions that are suitable for detection of APEH in infected erythrocytes.

To investigate the possibility of a physiological role for internalized APEH, we employed the APEH-selective inhibitor AA74-1 that was discovered in a library of triazole urea compound by Cravatt and colleagues (21). The exquisite selectivity of this covalent inhibitor for APEH has been demonstrated *in vitro* using mouse T cell lysates and *in situ* using cultured T cells (21). Furthermore, upon treatment of mouse T cells with AA74-1, the N-terminal acetylation state of

268 ~25 endogenous proteins was altered, which indicates that AA74-1 is able to engage its target *in*
269 *situ* (21). Thus, we considered AA74-1 to be an appropriate tool for the interrogation of APEH
270 function in *P. falciparum*. To validate the use of AA74-1 in the context of *P. falciparum*-infected
271 erythrocytes, we demonstrated by competitive ABPP that the inhibitor is highly selective for
272 parasite-internalized APEH in lysates of saponin-isolated parasites at concentrations below ~400
273 nM. It is also selective for APEH in uninfected erythrocytes (Fig. S1).
274 When AA74-1 was added to synchronized ring-stage parasites, inhibition of growth over
275 the first replication cycle required concentrations that were much higher than those needed to
276 inhibit APEH *in vitro*. However, a dramatic enhancement of potency was observed if the growth
277 inhibition experiment was continued for a second replication cycle, *i.e.* 96 hours. Notably, the
278 EC_{50} for growth inhibition after the second cycle was only 12-fold higher than the IC_{50} observed
279 for inhibition of APEH in competitive ABPP *in vitro*. Furthermore, the AA74-1 concentrations
280 that yielded efficient inhibition of growth replication were within the concentration range found
281 to be highly selective by competitive ABPP (*i.e.*, below 400 nM). Taken together, the evidence
282 strongly suggests that the growth defect observed during the second cycle is due to the selective
283 targeting of APEH.
284 Enhancement of drug potency during a second replication cycle is commonly observed
285 with inhibitors that target the parasite apicoplast (42). Our experiments with IPP
286 supplementation, however, revealed that internalized APEH is not acting in the context of the
287 apicoplast, nor is AA74-1 cross-inhibiting an apicoplast enzyme. Rather, it became clear from *in*
288 *vivo* experiments (*i.e.*, upon addition of AA74-1 to the medium of cultured parasites) that the
289 parasite-internalized APEH species were not inhibited by AA74-1 under these conditions. This
290 outcome was not due to its inability to penetrate the host cell: the erythrocyte pool of APEH was

quantitatively inhibited by AA74-1, both in uninfected erythrocytes and in the erythrocyte cytosol of infected cells. The reason for the recalcitrance of parasite-internalized APEH is not entirely clear. If APEH resides in the food vacuole, it will experience an acidic pH; however, we have demonstrated that the 55 kDa APEH species reacts with AA74-1 at pH 5.5 *in vitro*. It is possible that AA74-1 is not able to access the lumen of the food vacuole, or that it is inactivated inside the parasite by a hydrolytic enzyme. Whatever the reason, it is plausible that any parasite-internalized APEH that is present at the initiation of a growth inhibition experiment remains active throughout the replication cycle. The enhancement of potency during the following replication cycle could derive from the fact that the parasites invade erythrocytes containing AA74-1-inactivated APEH and therefore internalize inactive enzyme.

Our findings lead us to the intriguing idea that *P. falciparum* has adapted to use internalized APEH for a crucial metabolic function. The most apparent role for APEH, if as expected it resides in the food vacuole, is in catalyzing the hydrolysis of acetylated amino acids from the N-termini of peptides generated through the catabolism of endocytosed erythrocyte proteins. The two most abundant cytosolic proteins in the erythrocyte are hemoglobin (composed of α– and β–globin in the adult) and carbonic anhydrase-1, which are present at 97% and 1% of total protein, respectively (43). While α– and β–globin have not traditionally been thought to have acetylated N-termini, a proteome-wide analysis of erythrocyte proteins that explicitly addressed the acetylation status of N-termini found that the dominant species of both α– and β–globin are N-acetylated at a frequency of about 20% (44). Carbonic anhydrase-1 is known to possess an acetylated N-terminus (45). Furthermore, proteomic studies have identified over 1,500 soluble erythrocyte proteins (46, 47), around 53% of which are N-terminally acetylated (44). Given the large quantities of erythrocyte cytosol that are digested in the food vacuole, a

mechanism is likely needed for efficient removal of N-acetylated amino acids from peptides generated by endoproteolytic hydrolysis, as N-blocked peptides are expected to be poor substrates for the vacuolar exopeptidase dipeptidyl aminopeptidase 1 and the M1- and M24-family aminopeptidases PfA-M1 and PfAPP (48, 49). Although the pH optimum of human erythrocyte APEH is reported to be close to neutral pH (13, 50), TAMRA-FP labeling at pH 5.5 strongly suggests that parasite-internalized APEH retains catalytic activity, albeit diminished, at the acidic pH of the food vacuole. The co-internalization of host cell APEH could provide the parasite with an elegant solution for the need to catabolize N-acetylated peptides. Our findings lay the groundwork for further studies (such as metabolomic approaches) that could provide a direct test of this hypothesis.

MATERIALS AND METHODS

Reagents. The TAMRA-fluorophosphonate activity-based probe was obtained from ThermoFisher. *N*-(*trans*-epoxysuccinyl)-*L*-leucine 4-guanidinobutylamide (E-64), AA74-1, clindamycin, chloroquine and isopentenyl pyrophosphate trilithium salt were purchased from Sigma. Pepstatin A was purchased from MP biomedicals.

Parasite culture. *P. falciparum* 3D7 was cultured in human O^+ erythrocytes (Interstate Blood Bank, Memphis, TN) at 2% hematocrit in RPMI 1640 medium supplemented with 27 mM sodium bicarbonate, 11 mM glucose, 0.37 mM hypoxanthine, 10 µg/mL gentamicin, and 5 g/L Albumax I (Invitrogen). Unless otherwise indicated, cultures were incubated at 37 °C in a 5% CO_2 incubator. Cultures were synchronized by treatment with 5% (w/v) sorbitol (51).

337 **Preparation of parasite lysate**. Synchronized cultures of maturing parasites (32-40 h post-
338 invasion, hpi) were separated from soluble erythrocyte and parasitophorous vacuole proteins by
339 treatment with 0.03% (w/v) saponin in cold Dulbecco's phosphate-buffered saline (PBS, pH 7.4)
340 for 10 minutes on ice. Saponin-isolated parasites were recovered by centrifugation at 1940 x *g* at
341 4 °C for 10 minutes and were washed three times with cold PBS. The yield of parasites was
342 determined by counting on a hemocytometer. Parasites were suspended to a density of 5 x 10^8
343 parasites/mL in cold PBS containing the protease inhibitors pepstatin A (5 µM) and E-64 (10
344 µM). The parasite suspension was subjected to three rounds of sonication at 30% power for 10
345 seconds. After centrifugation at 17,000 x *g* to pellet cellular debris, aliquots of clarified lysates
346 were snap frozen in liquid N_2 and stored at – 80 °C.
347
348 **Preparation of uninfected erythrocyte lysate.** Uninfected erythrocytes were washed thrice in
349 cold PBS, counted on a hemocytometer and resuspended in cold PBS containing 5 µM pepstatin
350 and 10 µM E-64 to a density to 5 x 10^8 cells/mL. Lysates of resuspended erythrocytes were
351 prepared and stored as described above for saponin-isolate parasites.
352
353 **Activity-based protein profiling**. TAMRA-FP labeling reactions were conducted with 19.8 µL
354 of parasite or erythrocyte lysate, which corresponds to ~ 10^7 cells/reaction. To start the reaction,
355 0.2 µL of 100 µM TAMRA-FP was added, giving a final concentration of 1 µM. Reactions were
356 incubated at 30 °C for 30 minutes and then stopped by the addition of one volume of 2x reducing
357 SDS-PAGE loading buffer and incubation at 95 °C for 5 minutes. For competitive ABPP
358 experiments, inhibitor or vehicle (DMSO) was added and reactions were incubated for 20
359 minutes at 30 °C prior to the addition of TAMRA-FP. Labeled proteins were resolved on 8.5%

or 10% reducing SDS-polyacrylamide gels. In-gel TAMRA fluorescence was recorded on a Typhoon Trio flatbed scanner (GE Healthcare Life Sciences, Piscataway, NJ). Fluorescence profiles and peak volumes of labeled proteins were obtained using ImageQuant TL v2005 (GE Healthcare Life Sciences, Piscataway, NJ). For calculation of AA74-1 IC_{50} values (Fig. 2), the peak volume for the 55 kDa APEH species in saponin-isolated parasites was normalized to that of a ~160 kDa species (Fig. 2A, black asterisk) that was not inhibited by AA74-1 at any concentration. Normalization of erythrocyte APEH peak volumes was conducted in a similar manner (see Fig. S2). IC_{50} values were calculated by nonlinear regression fitting of the data to a four-parameter sigmoidal curve using KaleidaGraph 4.5 (Synergy software, Reading, PA).

Immunoblotting. Competitive ABPP on crude lysates from ~ 10^7 saponin-isolated parasites or uninfected erythrocytes was performed as described above. Following in-gel fluorescence scanning, proteins were transferred to a nitrocellulose membrane which was blocked with 2% bovine serum albumin in Tris-buffered saline containing 0.1% Tween 20 (TBST/BSA) for one hour at room temperature. The membrane was then incubated with primary antibody diluted in TBST/BSA for one hour followed by a one hour incubation with horseradish peroxidase-conjugated anti-rabbit secondary antibody (1:10,000, GE Healthcare life sciences, Piscataway, NJ). Primary antibodies used were: affinity purified anti-APEH rabbit polyclonal (IgG) raised against an APEH fragment consisting of amino acids 381-732 (product # 14758-1-AP, Proteintech, Rosemont, IL; 0.26 µg/mL) and affinity purified anti-PfA-M1 (0.13 µg/mL; (52)). Chemiluminescent signal was developed with ECL Plus (GE Healthcare life sciences, Piscataway, NJ) and recorded on x-ray film, which was digitized by scanning, or imaged on a ChemiDoc MP system (Bio-Rad laboratories, Hercules, CA). Image contrast for the TAMRA-FP

383 fluorescence and chemiluminescent signal was adjusted with Adobe Photoshop CS2 (Adobe,
384 Inc., San Jose, CA).
385
386 ***P. falciparum* growth inhibition assays.** Synchronized ring-stage cultures were seeded at 3%
387 parasitemia (48 h assay) or 0.6% parasitemia (96 h assay) and 1% hematocrit in a 96-well flat
388 bottom plate. Inhibitors were added from 1000x stock solutions in DMSO to generate two-fold
389 concentration series of AA74-1 (0.61 nM – 10 μM), chloroquine (1.9 – 250 nM) or clindamycin
390 (0.3 nM – 10 μM). After 48 or 96 h incubation at 37 °C under reduced oxygen conditions (5%
391 O_2, 5% CO_2, and 90% N_2), parasite growth was determined using a SYBR Green I DNA
392 quantitation assay as previously described (53). Values from samples containing 0.1% DMSO
393 were used to calculate relative SYBR Green fluorescence. Each assay was performed with two
394 technical replicates, which were averaged to generate a single biological replicate. EC_{50} values
395 were calculated by nonlinear regression fitting of the data to a four-parameter sigmoidal curve
396 using KaleidaGraph 4.5 (Synergy software, Reading, PA). Means and standard deviations from
397 three biological replicates are reported in Table 1. For experiments with 200 μM IPP
398 supplementation, single technical replicates were conducted for each biological replicate.
399
400 **AA74-1 inhibition of APEH *in vivo***. Trophozoite-stage parasites (30-38 hpi) or uninfected
401 erythrocytes were incubated in culture medium supplemented with AA74-1 (100 nM, 1 μM, or
402 10 μM) or with 0.1% DMSO for four hours at 37 °C under reduced oxygen conditions with
403 gentle mixing on an orbital rotator. Cultures were washed four times in cold RPMI to remove
404 exogenous AA74-1. Parasites were then isolated with saponin as described above. Saponin-
405 isolated parasites and uninfected erythrocytes were counted with a hemocytometer, resuspended

406 in cold PBS at a cell density of 5 x 10^8 per mL, and stored at –80 °C. Samples were assayed
407 directly by competitive ABPP.

408 To investigate the inhibition of APEH in the host and parasite compartments of infected
409 erythrocytes, a synchronized trophozoite culture was treated with AA74-1 (100 nM) or with
410 0.1% DMSO for four hours at 37 °C under reduced oxygen conditions. The culture was washed
411 four times in cold RPMI to remove AA74-1 and then resuspended in RPMI media. Parasitized
412 erythrocytes were purified from the culture on a MACS magnetic LD column (Miltenyi Biotech,
413 Gaithersburg, MD) following the manufacturer's instructions. Enriched parasitized RBCs
414 (pRBCs) were subjected to saponin treatment as described in the section "Preparation of parasite
415 lysate". Saponin-isolated parasites (pRBC pellet) and the supernatant containing soluble host
416 erythrocyte proteins (pRBC sup) were collected and stored at –80 °C. Samples were used
417 directly for competitive ABPP.
418
419 **Activity and inhibition of APEH at acidic pH.** Saponin-isolated parasites were split into two
420 aliquots and resuspended to a density of 5 x 10^8 parasites/mL in either PBS pH 7.4 or 100 mM
421 sodium 2-(*N*-morpholino)ethanesulfonate (MES) pH 5.5, both of which included 5 μM pepstatin
422 A and 10 μM E-64. Crude lysates were prepared as described in "Preparation of parasite lysate".
423 APEH activity and inhibition by AA74-1 were analyzed as described in "Activity-based protein
424 profiling", with the modification that TAMRA-FP incubation times up to 60 minutes were
425 employed for reactions conducted at pH 5.5. After fluorescence scanning, proteins were
426 immediately transferred to nitrocellulose and relative loading levels were assessed by
427 immunoblotting with an antibody against the *P. falciparum* aminopeptidase PfA-M1 (see
428 "Immunoblotting").

ACKNOWLEDGEMENTS

This work was supported by National Institute of Allergy and Infectious Diseases grant AI133136. The funding agency had no role in study design, data collection and interpretation, or the decision to submit the work for publication. R.E. and M.K. designed the experiments, R.E. and C.D. conducted the experiments, and R.E. and M.K. prepared the manuscript.

FIGURE LEGENDS

Figure 1: Identification of human APEH in saponin-isolated *P. falciparum*. (A) TAMRA-FP labeling of serine hydrolases in crude lysates of uninfected human erythrocytes (RBC) and saponin-isolated parasites (SAP). (B) Competitive ABPP using a panel of serine hydrolase inhibitors (1 μM) that target various classes of serine hydrolase (see Table S1) or vehicle (1% DMSO) control. The 80 and 55 kDa species that react quantitatively with AA74-1 are indicated with red asterisks. (C) Structure of the APEH-selective inhibitor AA74-1. (D) Effect of AA74-1 (1 μM) on TAMRA-FP labeling of serine hydrolases in a crude lysate of uninfected erythrocytes. The red asterisk indicates an 80 kDa species that is inhibited by AA74-1. (E) Immunodetection of human APEH. Left panel: TAMRA-FP profile of serine hydrolases in lysates of uninfected erythrocytes (RBC) and saponin-isolated parasites (SAP) with and without 1 μM AA74-1. Right panel: anti-APEH immunoblot following transfer of proteins to nitrocellulose. Red asterisks indicate AA74-1-inhibited species. Bands below 50 kDa in SAP lanes may represent APEH degradation products. Sizes of molecular markers are indicated in kDa.

Figure 2: *In vitro* potency and selectivity of AA74-1 for parasite-internalized APEH. (A) Competitive ABPP with AA74-1 over a concentration range of 0.06 – 405 nM. Upper panel: Saponin-isolated parasites (SAP). The 55 and 80 kDa APEH species are indicated with red asterisks. The species used for APEH peak volume normalization (see Materials and Methods) is indicated with a black asterisk. Lower panel: Uninfected erythrocytes (RBC). APEH is indicated with a red asterisk. See Fig. S2 for the full gel image and the species used for peak volume normalization. (B) Plot of normalized APEH peak volume, expressed as a fraction of the control ("0 nM", 1% DMSO), *vs.* AA74-1 concentration. Data are from the gel image in (A), which represents one of three biological replicates. Points were fit to a four-parameter sigmoidal curve. (C) Selectivity of AA74-1 in lysates of saponin-isolated parasites. TAMRA fluorescence profiles were generated for lanes in (A) corresponding to 0, 135 and 405 nM AA74-1. The 55 and 80 kDa internalized APEH species are indicated with red asterisks. Prodrug activation and resistance esterase is indicated with a blue asterisk. For A and C, the molecular masses of markers are indicated in kDa.

Figure 3: Effect of AA74-1 on parasite replication over two cycles. Concentration-response plots for parasites cultured in the presence of AA74-1 (A) or clindamycin (B) for 48 h (red circles), 96 h (blue circles) or 96 h in the presence of 200 μM IPP (green circles). At the indicated time points, parasite DNA was quantified using a SYBR Green I assay. Data are expressed as a percentage of the fluorescence value for the vehicle (DMSO) control. Inhibition curves were generated by non-linear regression fits to a four-parameter sigmoidal curve. The lower baselines are non-zero due to background fluorescence.

Figure 4: Analysis of AA74-1 inhibition of APEH *in vivo*. (A) Characterization of APEH inhibition upon AA74-1 treatment of cultured *P. falciparum*-infected or uninfected erythrocytes. Upper: Flow diagram of the experimental approach. Lower: TAMRA-FP labeling of saponin-isolated parasites (SAP) and uninfected erythrocytes (RBC) following *in vivo* treatment. (B) Characterization of *in vivo* APEH inhibition by AA74-1 in the infected erythrocyte cytosol and in saponin-isolated parasites. Upper: Flow diagram of the experimental approach. Lower: TAMRA-FP labeling of the saponin-isolated parasite pellet (pRBC pellet) or the saponin supernatant containing soluble host erythrocyte proteins (pRBC sup) obtained from highly purified infected erythrocytes following treatment with 100 nM AA74-1. In both (A) and (B), ABPP was conducted with and without 1 μM AA74-1 ("AA74-1 in ABPP") to identify APEH species (red asterisks). One biological replicate is shown out of two that yielded similar results. Molecular masses of markers are indicated in kDa.

Figure 5: APEH activity and inhibition by AA74-1 at acidic pH. Upper panel: ABPP of saponin-isolated parasite lysates at pH 5.5 and 7.4. Times of TAMRA-FP labeling reactions are indicated. Each reaction was conducted with and without 1 μM AA74-1 to identify APEH. Lower panel: anti-PfA-M1 immunoblot to indicate relative loading levels. Red asterisks indicate the 55 and 80 kDa internalized APEH species. Molecular masses of markers are indicated in kDa.

Figure S1: Competitive ABPP of uninfected erythrocyte lysate. APEH is indicated with a red asterisk. Inhibitor structures and selectivities are given in Table S1. Molecular masses of markers are indicated in kDa.

Figure S2: *In vitro* potency and selectivity of AA74-1 for erythrocyte APEH. The full gel corresponding to the segment in Fig. 2A is shown. APEH is indicated with a red asterisk and the species used for peak volume normalization is indicated with a black asterisk. Molecular masses of markers are indicated in kDa.

REFERENCES

1. World Health Organization. 2017. World Malaria Report 2018.
2. World Health Organization. 2013. World Malaria Report 2013.
3. Dondorp AM, Smithuis FM, Woodrow C, Seidlein LV. 2017. How to contain artemisinin- and multidrug-resistant falciparum malaria. Trends Parasitol 33:353-363.
4. Duru V, Witkowski B, Menard D. 2016. *Plasmodium falciparum* resistance to artemisinin derivatives and piperaquine: A major challenge for malaria elimination in Cambodia. Am J Trop Med Hyg 95:1228-1238.
5. Bachovchin DA, Cravatt BF. 2012. The pharmacological landscape and therapeutic potential of serine hydrolases. Nat Rev Drug Discov 11:52-68.
6. Long JZ, Cravatt BF. 2011. The metabolic serine hydrolases and their functions in mammalian physiology and disease. Chem Rev 111:6022-63.
7. Aurrecoechea C, Brestelli J, Brunk BP, Dommer J, Fischer S, Gajria B, Gao X, Gingle A, Grant G, Harb OS, Heiges M, Innamorato F, Iodice J, Kissinger JC, Kraemer E, Li W, Miller JA, Nayak V, Pennington C, Pinney DF, Roos DS, Ross C, Stoeckert CJ, Jr., Treatman C, Wang H. 2009. PlasmoDB: a functional genomic database for malaria parasites. Nucleic Acids Res 37:D539-43.

520 8. Niphakis MJ, Cravatt BF. 2014. Enzyme inhibitor discovery by activity-based protein
521 profiling. Annu Rev Biochem 83:341-77.
522 9. Liu Y, Patricelli MP, Cravatt BF. 1999. Activity-based protein profiling: the serine
523 hydrolases. Proc Natl Acad Sci USA 96:14694-9.
524 10. Patricelli MP, Giang DK, Stamp LM, Burbaum JJ. 2001. Direct visualization of serine
525 hydrolase activities in complex proteomes using fluorescent active site-directed probes.
526 Proteomics 1:1067-71.
527 11. Fujino T, Tada T, Hosaka T, Beppu M, Kikugawa K. 2000. Presence of oxidized protein
528 hydrolase in human cell lines, rat tissues, and human/rat plasma. J Biochem 127:307-13.
529 12. Jones WM, Manning JM. 1985. Acylpeptide hydrolase activity from erythrocytes.
530 Biochem Biophys Res Commun 126:933-40.
531 13. Schonberger OL, Tschesche H. 1981. N-Acetylalanine aminopeptidase, a new enzyme
532 from human erythrocytes. Hoppe Seylers Z Physiol Chem 362:865-73.
533 14. Witheiler J, Wilson DB. 1972. The purification and characterization of a novel peptidase
534 from sheep red cells. J Biol Chem 247:2217-21.
535 15. Tsunasawa S, Narita K, Ogata K. 1975. Purification and properties of acylamino acid-
536 releasing enzyme from rat liver. J Biochem 77:89-102.
537 16. Radhakrishna G, Wold F. 1989. Purification and characterization of an N-acylaminoacyl-
538 peptide hydrolase from rabbit muscle. J Biol Chem 264:11076-81.
539 17. Gade W, Brown JL. 1978. Purification and partial characterization of alpha-N-
540 acylpeptide hydrolase from bovine liver. J Biol Chem 253:5012-8.
541 18. Fujino T, Kojima M, Beppu M, Kikugawa K, Yasuda H, Takahashi K. 2000.
542 Identification of the cleavage sites of oxidized protein that are susceptible to oxidized

protein hydrolase (OPH) in the primary and tertiary structures of the protein. J Biochem 127:1087-93.

19. Yamin R, Zhao C, O'Connor PB, McKee AC, Abraham CR. 2009. Acyl peptide hydrolase degrades monomeric and oligomeric amyloid-beta peptide. Mol Neurodegener 4:33.

20. Perrier J, Durand A, Giardina T, Puigserver A. 2005. Catabolism of intracellular N-terminal acetylated proteins: involvement of acylpeptide hydrolase and acylase. Biochimie 87:673-85.

21. Adibekian A, Martin BR, Wang C, Hsu KL, Bachovchin DA, Niessen S, Hoover H, Cravatt BF. 2011. Click-generated triazole ureas as ultrapotent, in vivo-active serine hydrolase inhibitors. Nat Chem Biol 7:469-478.

22. Palmieri G, Bergamo P, Luini A, Ruvo M, Gogliettino M, Langella E, Saviano M, Hegde RN, Sandomenico A, Rossi M. 2011. Acylpeptide hydrolase inhibition as targeted strategy to induce proteasomal down-regulation. PLoS One 6:e25888.

23. Shimizu K, Kiuchi Y, Ando K, Hayakawa M, Kikugawa K. 2004. Coordination of oxidized protein hydrolase and the proteasome in the clearance of cytotoxic denatured proteins. Biochem Biophys Res Commun 324:140-6.

24. Beaumelle BD, Vial HJ, Philippot JR. 1987. Reevaluation, using marker enzymes, of the ability of saponin and ammonium chloride to free Plasmodium from infected erythrocytes. J Parasitol 73:743-8.

25. Jones WM, Scaloni A, Bossa F, Popowicz AM, Schneewind O, Manning JM. 1991. Genetic relationship between acylpeptide hydrolase and acylase, two hydrolytic enzymes

with similar binding but different catalytic specificities. Proc Natl Acad Sci USA 88:2194-8.

26. Yeh E, DeRisi JL. 2011. Chemical rescue of malaria parasites lacking an apicoplast defines organelle function in blood-stage *Plasmodium falciparum*. PLoS Biol 9:e1001138.

27. Dahl EL, Rosenthal PJ. 2007. Multiple antibiotics exert delayed effects against the *Plasmodium falciparum* apicoplast. Antimicrob Agents Chemother 51:3485-90.

28. Bennett TN, Kosar AD, Ursos LM, Dzekunov S, Singh Sidhu AB, Fidock DA, Roepe PD. 2004. Drug resistance-associated pfCRT mutations confer decreased *Plasmodium falciparum* digestive vacuolar pH. Mol Biochem Parasitol 133:99-114.

29. Klonis N, Tan O, Jackson K, Goldberg D, Klemba M, Tilley L. 2007. Evaluation of pH during cytostomal endocytosis and vacuolar catabolism of hemoglobin in *Plasmodium falciparum*. Biochem J 407:343-54.

30. Fairfield AS, Meshnick SR, Eaton JW. 1983. Malaria parasites adopt host cell superoxide dismutase. Science 221:764-766.

31. Bonday ZQ, Dhanasekaran S, Rangarajan PN, Padmanaban G. 2000. Import of host δ-aminolevulinate dehydratase into the malarial parasite: Identification of a new drug target. Nat Med 6:898-903.

32. Koncarevic S, Rohrbach P, Deponte M, Krohne G, Prieto JH, Yates III J, Rahlfs S, Becker K. 2009. The malarial parasite *Plasmodium falciparum* imports the human protein peroxiredoxin 2 for peroxide detoxification. Proc Natl Acad Sci USA 106:13323-13328.

586 33. Elliott DA, McIntosh MT, Hosgood HD, Chen S, Zhang G, Baevova P, Joiner KA. 2008.
587 Four distinct pathways of hemoglobin uptake in the malaria parasite *Plasmodium*
588 *falciparum*. Proc Natl Acad Sci USA 105:2463-8.
589 34. Lazarus MD, Schneider TG, Taraschi TF. 2008. A new model for hemoglobin ingestion
590 and transport by the human malaria parasite *Plasmodium falciparum*. J Cell Sci
591 121:1937-49.
592 35. Abu Bakar N, Klonis N, Hanssen E, Chan C, Tilley L. 2010. Digestive-vacuole genesis
593 and endocytic processes in the early intraerythrocytic stages of *Plasmodium falciparum*. J
594 Cell Sci 123:441-50.
595 36. Hanssen E, Knoechel C, Dearnley M, Dixon MW, Le Gros M, Larabell C, Tilley L.
596 2012. Soft X-ray microscopy analysis of cell volume and hemoglobin content in
597 erythrocytes infected with asexual and sexual stages of *Plasmodium falciparum*. J Struct
598 Biol 177:224-32.
599 37. Goldberg DE. 2005. Hemoglobin degradation. Curr Top Microbiol Immunol 295:275-91.
600 38. Scaloni A, Ingallinella P, Andolfo A, Jones W, Marino G, Manning JM. 1999. Structural
601 investigations on human erythrocyte acylpeptide hydrolase by mass spectrometric
602 procedures. J Protein Chem 18:349-60.
603 39. Sharma KK, Ortwerth BJ. 1993. Bovine lens acylpeptide hydrolase. Purification and
604 characterization of a tetrameric enzyme resistant to urea denaturation and proteolytic
605 inactivation. Eur J Biochem 216:631-7.
606 40. Durand A, Villard C, Giardina T, Perrier J, Juge N, Puigserver A. 2003. Structural
607 properties of porcine intestine acylpeptide hydrolase. J Protein Chem 22:183-91.

608 41. Chongcharoen K, Sharma KK. 1998. Characterization of trypsin-modified bovine lens
609 acylpeptide hydrolase. Biochem Biophys Res Commun 247:136-41.
610 42. McFadden GI, Roos DS. 1999. Apicomplexan plastids as drug targets. Trends Microbiol
611 7:328-33.
612 43. Ringrose JH, van Solinge WW, Mohammed S, O'Flaherty MC, van Wijk R, Heck AJ,
613 Slijper M. 2008. Highly efficient depletion strategy for the two most abundant
614 erythrocyte soluble proteins improves proteome coverage dramatically. J Proteome Res
615 7:3060-3.
616 44. Lange PF, Huesgen PF, Nguyen K, Overall CM. 2014. Annotating N termini for the
617 human proteome project: N termini and Nalpha-acetylation status differentiate stable
618 cleaved protein species from degradation remnants in the human erythrocyte proteome. J
619 Proteome Res 13:2028-44.
620 45. Lin KT, Deutsch HF. 1973. Human carbonic anhydrases. XI. The complete primary
621 structure of carbonic anhydrase B. J Biol Chem 248:1885-93.
622 46. Bryk AH, Wisniewski JR. 2017. Quantitative analysis of human red blood cell proteome.
623 J Proteome Res 16:2752-2761.
624 47. Roux-Dalvai F, Gonzalez de Peredo A, Simo C, Guerrier L, Bouyssie D, Zanella A,
625 Citterio A, Burlet-Schiltz O, Boschetti E, Righetti PG, Monsarrat B. 2008. Extensive
626 analysis of the cytoplasmic proteome of human erythrocytes using the peptide ligand
627 library technology and advanced mass spectrometry. Mol Cell Proteomics 7:2254-69.
628 48. Dalal S, Klemba M. 2007. Roles for two aminopeptidases in vacuolar hemoglobin
629 catabolism in *Plasmodium falciparum*. J Biol Chem 282:35978-87.

630 49. Klemba M, Gluzman I, Goldberg DE. 2004. A *Plasmodium falciparum* dipeptidyl
631 aminopeptidase I participates in vacuolar hemoglobin degradation. J Biol Chem
632 279:43000-43007.
633 50. Jones WM, Manning JM. 1988. Substrate specificity of an acylaminopeptidase that
634 catalyzes the cleavage of the blocked amino termini of peptides. Biochim Biophys Acta
635 953:357-60.
636 51. Lambros C, Vanderberg JP. 1979. Synchronization of *Plasmodium falciparum*
637 erythrocytic stages in culture. J Parasitol 65:418-20.
638 52. Ragheb D, Dalal S, Bompiani KM, Ray WK, Klemba M. 2011. Distribution and
639 biochemical properties of an M1-family aminopeptidase in *Plasmodium falciparum*
640 indicate a role in vacuolar hemoglobin catabolism. J Biol Chem 286:27255-65.
641 53. Smilkstein M, Sriwilaijaroen N, Kelly JX, Wilairat P, Riscoe M. 2004. Simple and
642 inexpensive fluorescence-based technique for high-throughput antimalarial drug
643 screening. Antimicrob Agents Chemother 48:1803-6.
644

Table 1: EC_{50} values from *P. falciparum* growth inhibition assays. Values are means ± SD from three biological replicates. ND, not determined.

Compound	48 h EC_{50} (nM)	96 h EC_{50} (nM)	
		-IPP	+IPP
AA74-1	>1,000	96 ± 38	94 ± 39
Clindamycin	>10,000	37 ± 24	>10,000
Chloroquine	9.0 ± 2.4	8.5 ± 2.0	ND

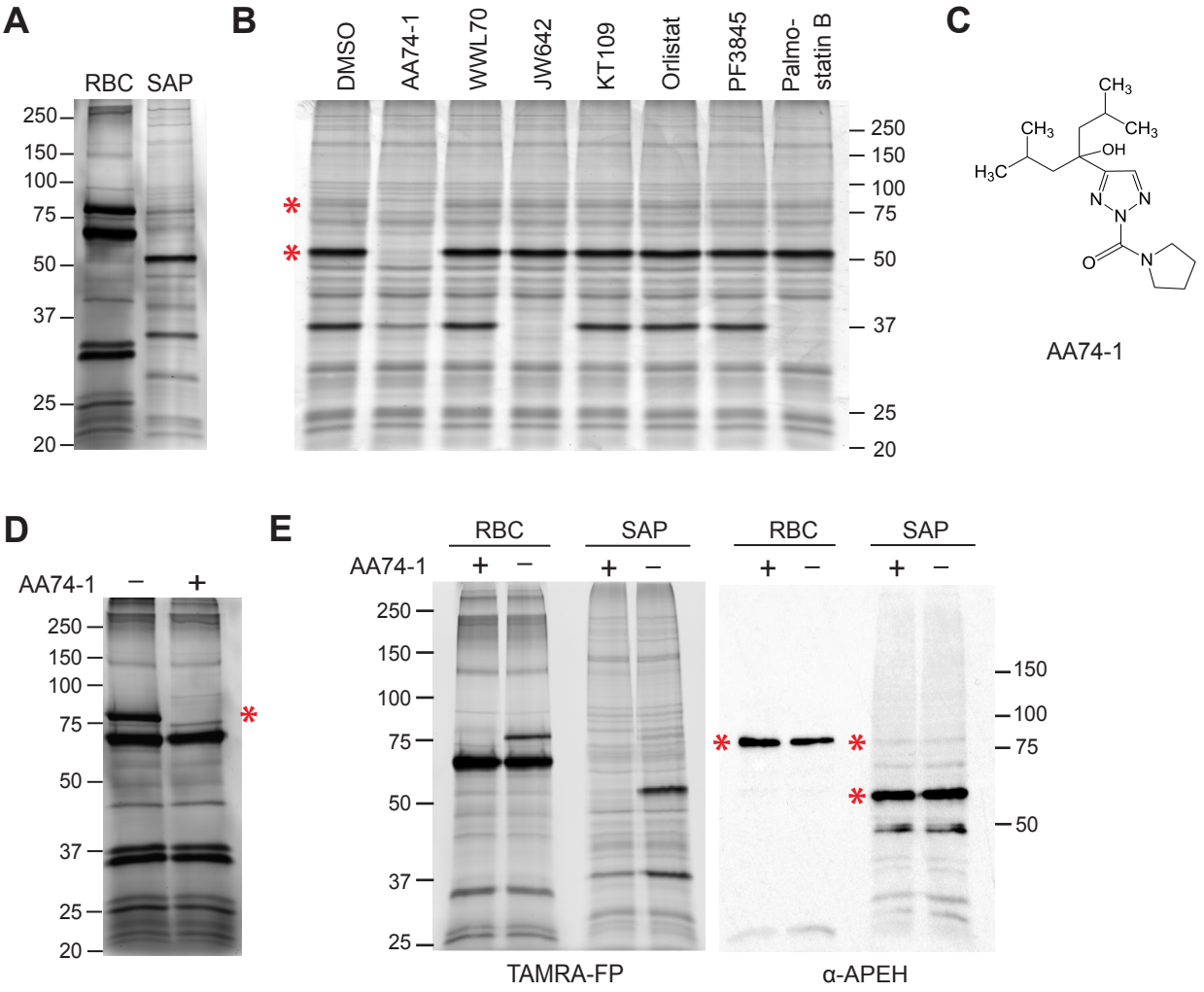

Figure 1: Identification of human APEH in saponin-isolated P. falciparum. (A) TAMRA-FP labeling of serine hydrolases in crude lysates of uninfected human erythrocytes (RBC) and saponin-isolated parasites (SAP). (B) Competitive ABPP using a panel of serine hydrolase inhibitors (1 μM) that target various classes of serine hydrolase (see Table S1) or vehicle (1% DMSO) control. The 80 and 55 kDa species that react quantitatively with AA74-1 are indicated with red asterisks. (C) Structure of the APEH-selective inhibitor AA74-1. (D) Effect of AA74-1 (1 μM) on TAMRA-FP labeling of serine hydrolases in a crude lysate of uninfected erythrocytes. The red asterisk indicates an 80 kDa species that is inhibited by AA74-1. (E) Immunodetection of human APEH. Left panel: TAMRA-FP profile of serine hydrolases in lysates of uninfected erythrocytes (RBC) and saponin-isolated parasites (SAP) with and without 1 μM AA74-1. Right panel: anti-APEH immunoblot following transfer of proteins to nitrocellulose. Red asterisks indicate AA74-1-inhibited species. Bands below 50 kDa in SAP lanes may represent APEH degradation products. Sizes of molecular markers are indicated in kDa.

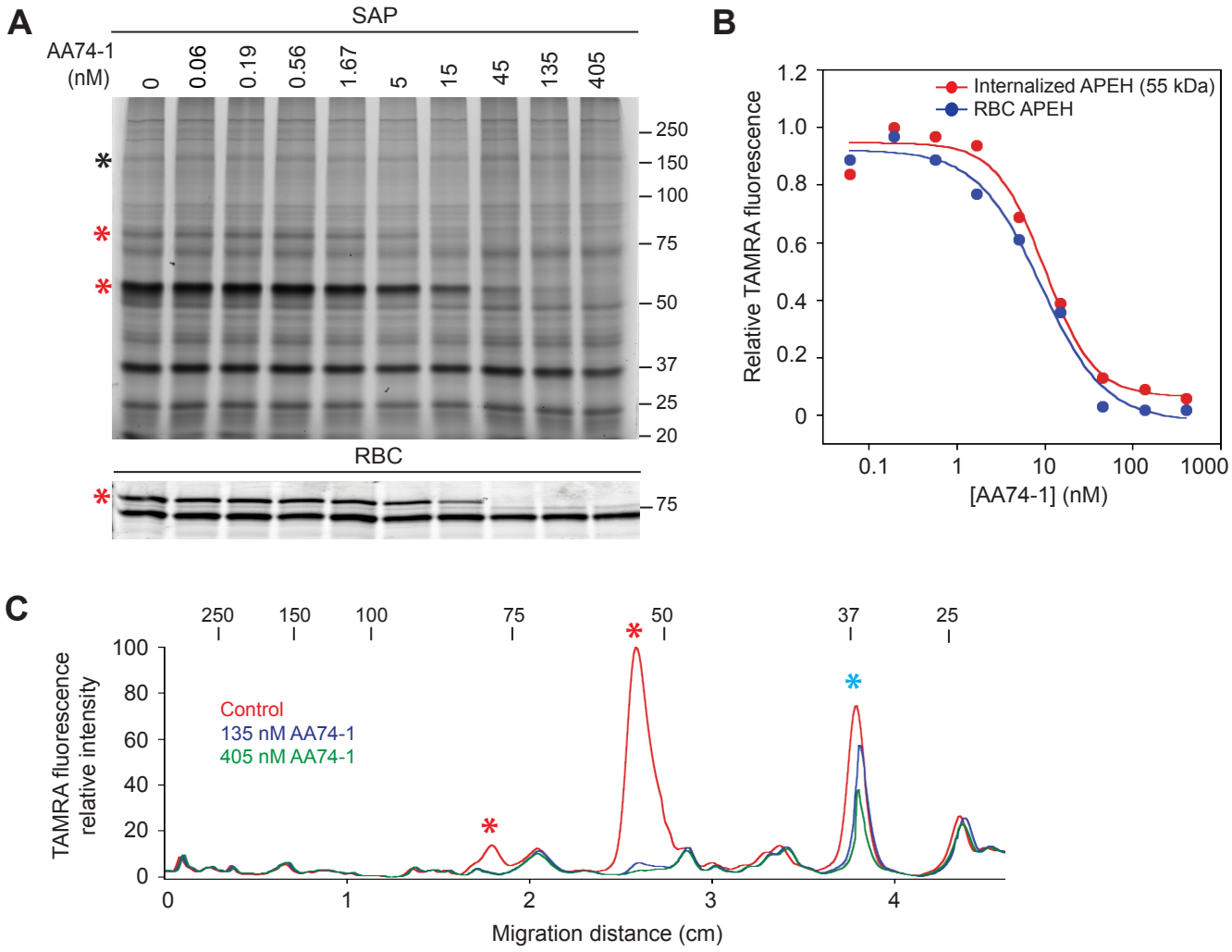

Figure 2: *In vitro* potency and selectivity of AA74-1 for parasite-internalized APEH. (A) Competitive ABPP with AA74-1 over a concentration range of 0.06 – 405 nM. Upper panel: Saponin-isolated parasites (SAP). The 55 and 80 kDa APEH species are indicated with red asterisks. The species used for APEH peak volume normalization (see Materials and Methods) is indicated with a black asterisk. Lower panel: Uninfected erythrocytes (RBC). APEH is indicated with a red asterisk. See Fig. S2 for the full gel image and the species used for peak volume normalization. (B) Plot of normalized APEH peak volume, expressed as a fraction of the control ("0 nM", 1% DMSO), vs. AA74-1 concentration. Data are from the gel image in (A), which represents one of three biological replicates. Points were fit to a four-parameter sigmoidal curve. (C) Selectivity of AA74-1 in lysates of saponin-isolated parasites. TAMRA fluorescence profiles were generated for lanes in (A) corresponding to 0, 135 and 405 nM AA74-1. The 55 and 80 kDa internalized APEH species are indicated with red asterisks. Prodrug activation and resistance esterase is indicated with a blue asterisk. For A and C, the molecular masses of markers are indicated in kDa.

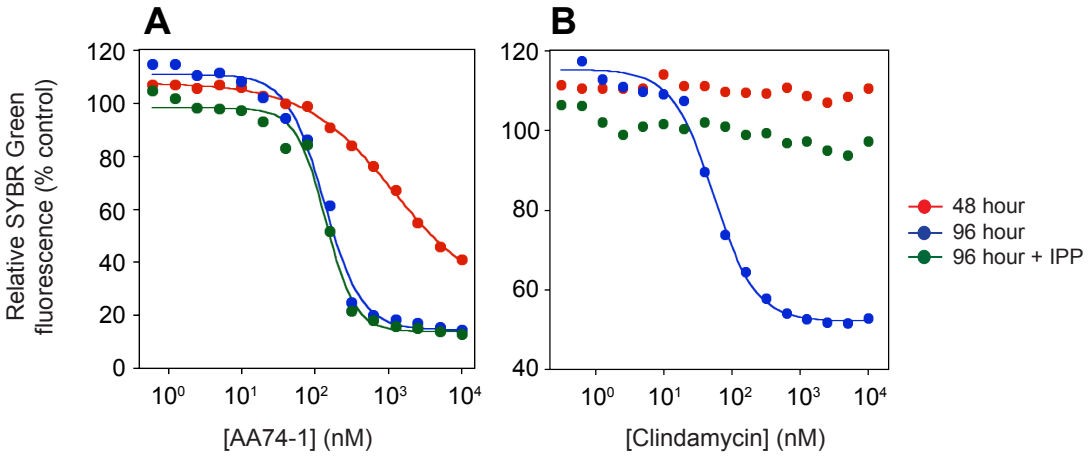

Figure 3: Effect of AA74-1 on parasite replication over two cycles. Concentration-response plots for parasites cultured in the presence of AA74-1 (A) or clindamycin (B) for 48 h (red circles), 96 h (blue circles) or 96 h in the presence of 200 μM IPP (green circles). At the indicated time points, parasite DNA was quantified using a SYBR Green I assay. Data are expressed as a percentage of the fluorescence value for the vehicle (DMSO) control. Inhibition curves were generated by non-linear regression fits to a four-parameter sigmoidal curve. The lower baselines are non-zero due to background fluorescence.

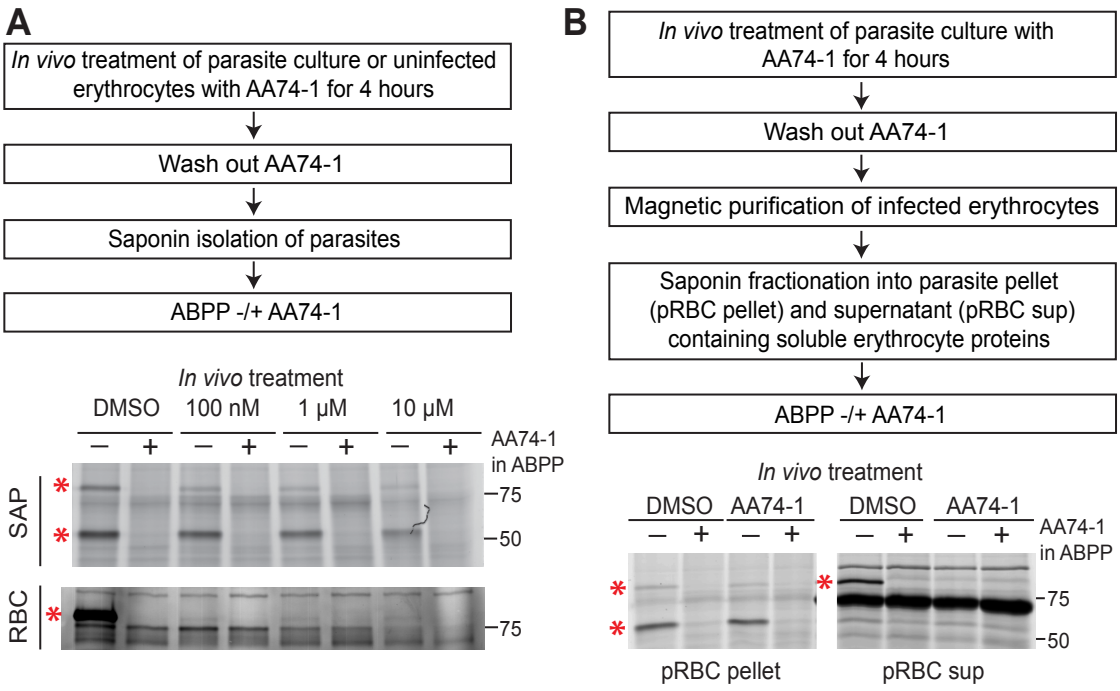

Figure 4: Analysis of AA74-1 inhibition of APEH *in vivo*. (A) Characterization of APEH inhibition upon AA74-1 treatment of cultured *P. falciparum*-infected or uninfected erythrocytes. Upper: Flow diagram of the experimental approach. Lower: TAMRA-FP labeling of saponin-isolated parasites (SAP) and uninfected erythrocytes (RBC) following *in vivo* treatment. (B) Characterization of *in vivo* APEH inhibition by AA74-1 in the infected erythrocyte cytosol and in saponin-isolated parasites. Upper: Flow diagram of the experimental approach. Lower: TAMRA-FP labeling of the saponin-isolated parasite pellet (pRBC pellet) or the saponin supernatant containing soluble host erythrocyte proteins (pRBC sup) obtained from highly purified infected erythrocytes following treatment with 100 nM AA74-1. In both (A) and (B), ABPP was conducted with and without 1 µM AA74-1 ("AA74-1 in ABPP") to identify APEH species (red asterisks). One biological replicate is shown out of two that yielded similar results. Molecular masses of markers are indicated in kDa.

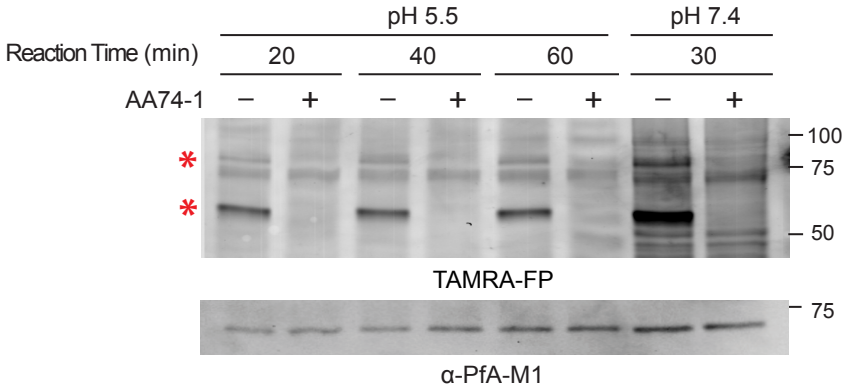

Figure 5: APEH activity and inhibition by AA74-1 at acidic pH. Upper panel: ABPP of saponin-isolated parasite lysates at pH 5.5 and 7.4. Times of TAMRA-FP labeling reactions are indicated. Each reaction was conducted with and without 1 μM AA74-1 to identify APEH. Lower panel: anti-PfA-M1 immunoblot to indicate relative loading levels. Red asterisks indicate the 55 and 80 kDa internalized APEH species. Molecular masses of markers are indicated in kDa.

Table S1: Serine hydrolase inhibitors used in this study for competitive activity-based protein profiling.

Inhibitor	Structure	Target	Ref
AA74-1	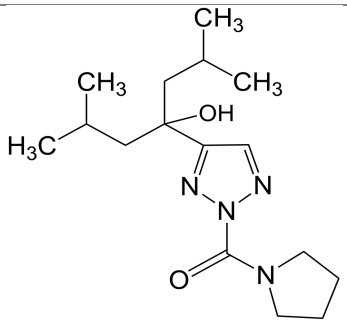	acylpeptide hydrolase	(1)
WWL70	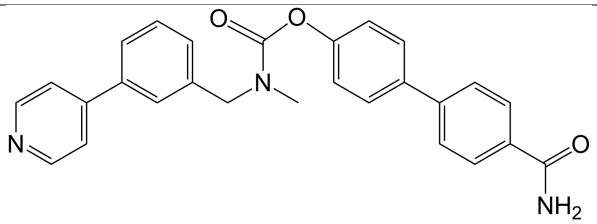	α/β-hydrolase domain 6	(2)
JW642	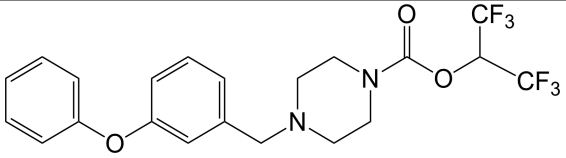	monoacylglycerol lipase	(3)
KT109	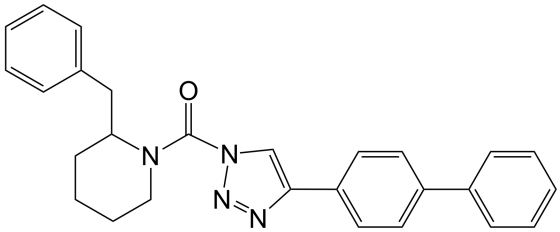	diacylglycerol lipase	(4)
Orlistat	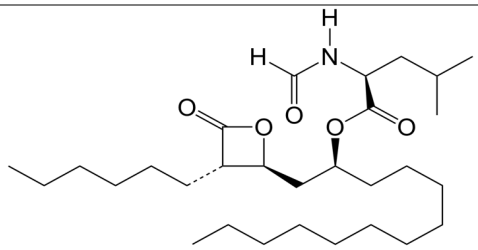	triacylglycerol lipase	(5)
PF3845	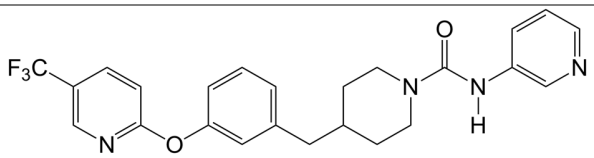	fatty acid amide hydrolase	(6)
Palmostatin B	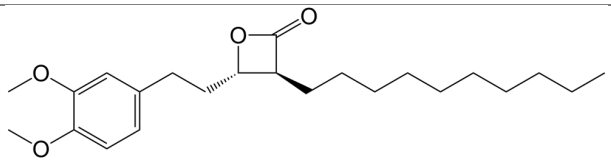	thioesterase	(7)

REFERENCES

1. Adibekian A, Martin BR, Wang C, Hsu KL, Bachovchin DA, Niessen S, Hoover H, Cravatt BF. 2011. Click-generated triazole ureas as ultrapotent, *in vivo*-active serine hydrolase inhibitors. Nat Chem Biol 7:469-478.

2. Blankman JL, Simon GM, Cravatt BF. 2007. A comprehensive profile of brain enzymes that hydrolyze the endocannabinoid 2-arachidonoylglycerol. Chem Biol 14:1347-56.

3. Chang JW, Niphakis MJ, Lum KM, Cognetta AB, 3rd, Wang C, Matthews ML, Niessen S, Buczynski MW, Parsons LH, Cravatt BF. 2012. Highly selective inhibitors of monoacylglycerol lipase bearing a reactive group that is bioisosteric with endocannabinoid substrates. Chem Biol 19:579-88.

4. Hsu KL, Tsuboi K, Adibekian A, Pugh H, Masuda K, Cravatt BF. 2012. DAGLbeta inhibition perturbs a lipid network involved in macrophage inflammatory responses. Nat Chem Biol 8:999-1007.

5. Hadvary P, Lengsfeld H, Wolfer H. 1988. Inhibition of pancreatic lipase *in vitro* by the covalent inhibitor tetrahydrolipstatin. Biochem J 256:357-61.

6. Ahn K, Johnson DS, Mileni M, Beidler D, Long JZ, McKinney MK, Weerapana E, Sadagopan N, Liimatta M, Smith SE, Lazerwith S, Stiff C, Kamtekar S, Bhattacharya K, Zhang Y, Swaney S, Van Becelaere K, Stevens RC, Cravatt BF. 2009. Discovery and characterization of a highly selective FAAH inhibitor that reduces inflammatory pain. Chem Biol 16:411-20.

7. Dekker FJ, Rocks O, Vartak N, Menninger S, Hedberg C, Balamurugan R, Wetzel S, Renner S, Gerauer M, Scholermann B, Rusch M, Kramer JW, Rauh D, Coates GW, Brunsveld L, Bastiaens PI, Waldmann H. 2010. Small-molecule inhibition of APT1 affects Ras localization and signaling. Nat Chem Biol 6:449-56.

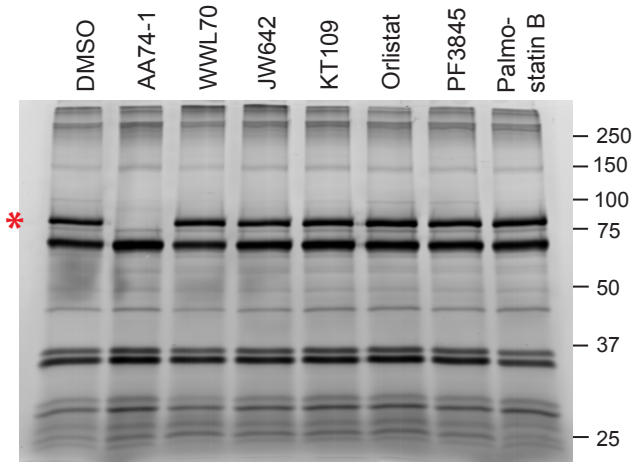

Figure S1: Competitive ABPP of uninfected erythrocyte lysate. APEH is indicated with a red asterisk. Inhibitor structures and selectivities are given in Table S1. Molecular masses of markers are indicated in kDa.

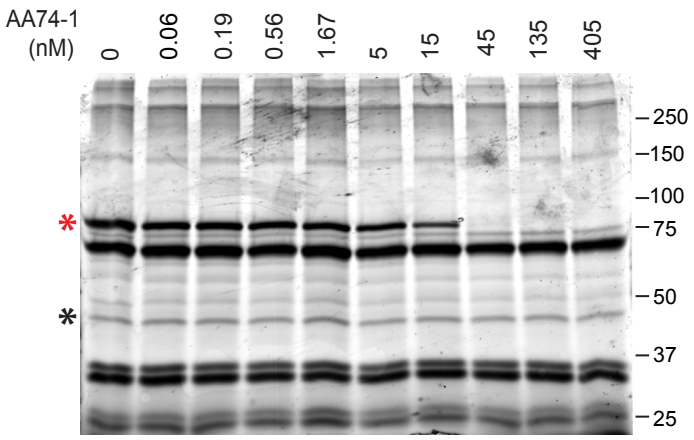

Figure S2: *In vitro* potency and selectivity of AA74-1 for erythrocyte APEH. The full gel corresponding to the segment in Fig. 2A is shown. APEH is indicated with a red asterisk and the species used for peak volume normalization is indicated with a black asterisk. Molecular masses of markers are indicated in kDa.